Basal and prism dislocation cores in magnesium: comparison of first-principles and embedded-atom-potential methods predictions

J A Yasi[1], T Nogaret[2], D R Trinkle[3], Y Qi[4], L G Hector Jr[4] and W A Curtin[2]

[1] Department of Physics, University of Illinois at Urbana-Champaign, Urbana, IL 61801, USA
[2] Division of Engineering, Brown University, Providence, RI 02912, USA
[3] Department of Material Science and Engineering, University of Illinois at Urbana-Champaign, Urbana, IL 61801, USA
[4] General Motors R&D Center, 30500 Mound Road, Warren, MI 48090-9055, USA

Abstract
The core structures of screw and edge dislocations on the basal and prism planes in Mg, and the associated gamma surfaces, were studied using an *ab initio* method and the embedded-atom-method interatomic potentials developed by Sun *et al* and Liu *et al*. The *ab initio* calculations predict that the basal plane dislocations dissociate into partials split by 16.7 Å (edge) and 6.3 Å (screw), as compared with 14.3 Å and 12.7 Å (Sun and Liu edge), and 6.3 Å and 1.4 Å (Sun and Liu screw), with the Liu screw dislocation being metastable. In the prism plane, the screw and edge cores are compact and the edge core structures are all similar, while *ab initio* does not predict a stable prismatic screw in stress-free conditions. These results are qualitatively understood through an examination of the gamma surfaces for interplanar sliding on the basal and prism planes. The Peierls stresses at $T = 0$ K for basal slip are a few megapascals for the Sun potential, in agreement with experiments, but are ten times larger for the Liu potential. The Peierls stresses for prism slip are 10–40 MPa for both potentials. Overall, the dislocation core structures from *ab initio* are well represented by the Sun potential in all cases while the Liu potential shows some notable differences. These results suggest that the Sun potential is preferable for studying other dislocations in Mg, particularly the $\langle c + a \rangle$ dislocations, for which the core structures are much larger and not accessible by *ab initio* methods.

1. Introduction

Magnesium alloys are being actively developed for structural applications due to their light weight [1]. However, the formability of Mg is poor due to its hexagonal close packed

Table 1. SFEs in Mg from interatomic potentials, *ab initio* calculations and experiments. The prism unstable SFEs are taken along the $\langle 1\,1\,-2\,0 \rangle$ direction.

Stacking fault energy (mJ m^{-2})		0001		1010	
		Stable	Unstable	Stable	Unstable
Igarashi 1990 [7]	FS EAM	10		155	
Liang 1986 [3]	Na56 pair	13.5	43	*X*	30.2
Present study	*Ab initio*	34	>92		218
Datta 2008 [28]	*Ab initio*	29.2	58.2		71.8
Jelinek 2007 [29]	*Ab initio*	37			
Smith 2006 [30]	*Ab initio*	20	108		265
Uesugi 2003 [31]	*Ab initio*	32	93		255
Gotsis 2002 [32]	*Ab initio*	16	116		
Chetty 1997 [33]	*Ab initio*	44			
Legrand 1985 [34]	*Ab initio*	30			
Couret 1985 [35]	Experiment	<50			
Fleischer 1986 [36]	Experiment	>90			
Fleischer 1986 [37]	Experimental review	280, 125, 102 and 74			
Devlin 1974 [38]	Experiment	60			

(HCP) structure: deformation occurs easily along the $\langle a \rangle$ axis via glide of $\langle a \rangle$ dislocations on the (1 0 0 0) basal and the stronger prism (1-100) planes but deformation is difficult along the $\langle c \rangle$ axis because the motion of both $\langle c + a \rangle$ dislocations and twinning dislocations in pyramidal planes requires high stress levels. Plastic deformation along the pyramidal plane directions is not well understood and constitutes a significant challenge for materials scientists. Because many aspects of plastic flow are associated with dislocation core structures, atomistic simulations are a natural starting point for investigating the problem.

There is a long history of atomistic work on dislocations in various HCP materials, but much of it does not pertain specifically to Mg. To date, only two interatomic potentials designed for Mg have been used to study Mg dislocations. The 'na56' pair-wise potential [2] was used to study $\langle a \rangle$ dislocations in the basal and prism planes and $\langle c+a \rangle$ dislocations [3–5] and twinning dislocations [6] in the pyramidal planes. The Finnis–Sinclair embedded-atom-method (EAM) potential [7] was fit to Mg experimental data (c/a ratio, the five elastic constants, the vacancy formation energy, the cohesion energies and the energy of the I2 stacking fault that results from slip of $1/3\langle 1 -1\,0\,0 \rangle$), and was used to study screw $\langle a \rangle$ dislocations in the basal and prism planes [8] and twinning dislocations [6]. These potentials have I2 stacking fault energy (SFE) values of ~ 10 mJ m^{-2}, which is much lower than the value of ~ 30 mJ m^{-2} obtained from *ab initio* calculations (see table 1). In addition, the Peierls stresses for dislocation motion in the basal plane is ~ 18 MPa for the na56, which is ~ 30 times larger than the experimental values. EAM potentials with larger I2 SFEs were developed for Mg by Liu *et al* [9] and Sun *et al* [10]. These two EAM potentials were fit to more physical properties than the previous potentials, but also to sets of forces from *ab initio* calculations using the force matching method [11]. The Sun potential was also improved by fitting additional parameters: the melting temperature T_m, the relative energies of FCC, BCC and HCP lattices between 0 K and T_m and the fluctuation amplitudes for five solid/liquid interface orientations. However, the dislocation core structures for these potentials have not been reported.

Bulk magnesium has been studied by first-principles methods, and table 1 summarizes the literature on the predicted SFEs. First-principles studies of dislocation core structures in metals are less common, but are now emerging more frequently due to the use of flexible boundary

condition methods. The lattice Green function (LGF) update method produces 'flexible' boundary conditions—where the atomistic geometry of a defect is directly coupled to the long-range strain field response of the surrounding material [12–14]. The flexible coupling allows calculations of defect geometries and properties using a much smaller number of atoms than the traditional 'supercell' approach (where the simulation cell is periodically repeated in all three dimensions). New techniques have made calculation and error estimation of the LGF efficient for density-functional theory [15, 16], and have successfully computed dislocation core structures in metals such as Al [17].

In this paper, we investigate dislocation structures in the basal and prism planes of Mg using the *ab initio*/LGF method and the Liu *et al* and Sun *et al* EAM potentials. We make quantitative comparisons among all the three systems for selected gamma surfaces, dislocation cores and Peierls stresses. The first-principles quantum results represent a baseline structure for future study of alloying effects, cross-slip and other phenomena. The EAM results demonstrate that the potential of Sun *et al* is generally superior to that of Liu *et al* in that it predicts structures and stresses in better agreement with first principles and experimental results. The results here justify the use of the Sun *et al* potential for the subsequent study of the important $\langle c + a \rangle$ and twinning dislocations, which will be reported on separately. The cores of the $\langle c + a \rangle$ dislocations are quite complex, spatially extended and subject to reconfiguration under the action of applied loads, such that first-principles methods for the $\langle c + a \rangle$ dislocations are not computationally feasible and semi-empirical approaches are necessary for gaining insight into non-basal plasticity in Mg.

This paper is organized as follows. In section 2, we describe the simulation geometries and methods. In sections 3 and 4, we present results for the screw and edge dislocations in the basal and prism planes, respectively. We discuss our results further and conclude in section 5.

2. Simulation geometries and methods

The simulation cells for all our studies use a Z coordinate normal to the glide plane and a Y coordinate parallel to the Burgers vector. We considered two different HCP crystal orientations. In standard HCP crystallographic notation, the basal orientation has $X = [1 -1 0 0]$, $Y = [1 1 -2 0]$, $Z = [0 0 0 1]$ while the prism orientation has $X = [0 0 0 1]$, $Y = [1 1 -2 0]$, $Z = [1 -1 0 0]$.

Gamma surfaces are computed as follows. The surfaces along the Z direction are free and periodic boundary conditions are applied along X and Y. The upper half of the crystal ($Z > 0$) is shifted by a translation vector $t = \mathbf{d}X + \mathbf{d}Y$ in the X–Y plane. All atoms are held fixed in the X and Y directions but are allowed to relax along the Z direction. The gamma surface then corresponds to the relaxed energy versus translation t. For EAM calculations, perfect crystals of dimensions $(1 \times 1 \times 19)$ and $(1 \times 1 \times 18)$ unit cells are created for the basal and prism cases. The 'quench method' was used to find the minimum energy [18], with convergence corresponding to individual forces below 10^{-8} eV A^{-1} on all interior atoms and below 10^{-6} eV A^{-1} on all atoms within the EAM potential cut-off radius from the free surfaces.

The *ab initio* calculations are performed with VASP [19, 20], a planewave-based density-functional theory code using Vanderbilt-type ultrasoft-pseudopotentials [21, 22] and the generalized-gradient approximation of Perdew and Wang for the exchange-correlation potential [23]. The 3s states of Mg are treated as valence electrons, while the other electron states are frozen in their core configurations; a planewave energy cut-off of 138 eV is used throughout the calculations. The choice of exchange-correlation potential, pseudopotential and planewave cut-off are made by comparing lattice and elastic constants and phonons spectra with experimental values; our selection produces errors of 0.7% for lattice constants, 5% for

bulk modulus and 3% for phonon frequencies. Gamma-surface calculations are performed using $1 \times 1 \times 9$ (18 layers) and $1 \times 1 \times 5$ (10 layers) periodic supercells for the basal and prism cases and relaxed perpendicular to the gamma-surface plane, and using 34×34 (basal) and 34×18 (prism) k-point meshes in the plane with a Methfessel–Paxton smearing of 0.2 eV. All forces are relaxed to within 5 meV Å^{-1}, corresponding to an energy error of less than 1%.

Computing isolated (stress-free) dislocation cores in *ab initio* requires careful construction of the simulation cell and associated LGF. Periodic boundary conditions are used along the dislocation line as for the EAM calculations; 16 (basal screw and prismatic edge) or 12 (basal edge) k-points along the dislocation line with a smearing of 0.5 eV provide for an accurate representation of the electronic density of states. The slip and long-range strain fields introduced by a dislocation are incompatible with periodic boundary conditions perpendicular to the dislocation line; flexible boundary conditions remedy this by using free surfaces away from the dislocation core, and using the bulk LGF to relax atoms as if they were embedded in bulk. For all dislocations, the atoms immediately around the core (region I) are relaxed using *ab initio* forces with a conjugate-gradient, the *ab initio* forces on the next outer region (region II) are relaxed using the LGF and the outermost atoms (region III) are updated from the LGF, giving flexible boundary conditions that eliminate the influence of free surfaces [14]. The basal screw dislocation relaxation requires 525 atoms (I: 54, II: 164, III: 307), the basal edge requires 806 atoms (I: 130, II: 247, III: 429) and the prismatic edge requires 465 atoms (I: 57, II: 118, III: 290); the sizes are commensurate with the amount of core spreading anticipated. The forces on atoms in regions I and II are relaxed iteratively until they are below 5 meV Å^{-1}, corresponding to errors in atomic positions of less than 5 mÅ. The LGF is derived from the force-constant matrix calculated with the direct-force method in a $6 \times 6 \times 4$ HCP supercell; as stated above, the harmonic response agrees with experimental phonon measurements to 3%.

In the atomistic simulations, dislocations are created in the centre of a perfect crystal having dimensions of one unit cell length along the line direction and $\sim$100 nm in the dislocation glide and Z directions. For the edge dislocation, one half-plane of atoms is removed and the remaining atoms are displaced according to the Volterra solution. For screw dislocations, the atoms are displaced according to the Volterra solution corresponding to two $1/2\langle a \rangle$ Burgers screw dislocations separated by a small distance ($1.5a$) along the glide plane. Boundary conditions for the EAM calculations are periodic in the dislocation line direction, the surface normal to the glide direction is free and the surface normal to the Z direction has mixed boundary conditions. Specifically, atoms located within the EAM potential cut-off radius of the Z surfaces are fixed in the Z direction, but have applied forces in X and Y to create shear stresses σ_{YZ} and/or σ_{XZ} when desired. Increments of applied stress are always smaller than 10% of the Peierls stress.

3. Results for basal plane slip

The gamma surfaces along the $[1 -1\,0\,0]$ direction between 0 and the I2 stable SF are shown in figure 1 for the *ab initio* calculations and Sun and Liu EAM potentials and the corresponding stable and unstable SFE energies are given in table 2. The stable SFE energies are all in the range of previous *ab initio* values and much larger than those from earlier potentials, with the Sun potential in better agreement with this *ab initio* result. The unstable SFE from *ab initio* is >92 mJ m^{-2} because energies were calculated only for the fault vectors ($0.166\langle 1 -1\,0\,0\rangle$ and $1/3\langle 1 -1\,0\,0\rangle$). The Sun and Liu potentials yield values in this range, 82 mJ m^{-2} and 117 mJ m^{-2}, respectively, but give different positions for the unstable point ($0.225\langle 1 -1\,0\,0\rangle$ versus $0.187\langle 1 -1\,0\,0\rangle$).
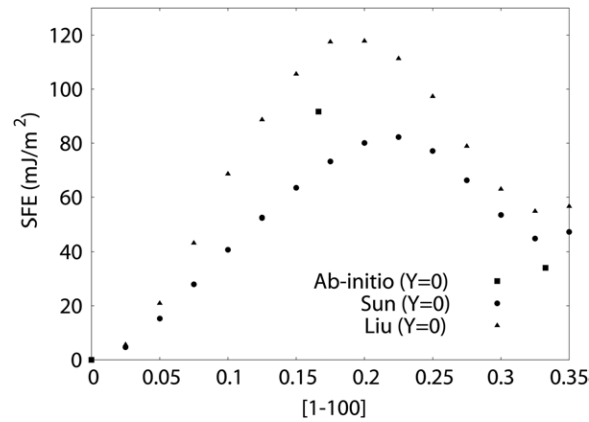
Figure 1. Basal plane gamma surfaces along the $[1 -1 0 0]$ direction between 0 and the I2 stable SF.

Table 2. Stable and unstable SFEs (mJ m^{-2}) in the basal and prism planes, and the ratio basal/prism unstable SFEs for *ab initio* calculations, Sun and Liu EAM potentials. The prism unstable SFEs are given along the minimum energy path and along the $\langle 1 1 -2 0 \rangle$ direction.

Stacking fault energy (mJ m^{-2})	Basal		Prism			Ratio basal/prism unstable SFEs
	Stable	Unstable	Stable	Unstable (minimum path)	Unstable ($\langle 1 1 -2 0 \rangle$)	
Ab initio	34	>92	218	218	218	0.42
Sun EAM	44	82	132	152	170	0.62
Liu EAM	54	117	117	129	132	0.91

The edge and screw dislocation core structures are shown using both a differential displacement (DD) plot and contours of the Nye tensor in figures 2 and 3, respectively, for the *ab initio* and Sun potential calculations. The arrows in figures 2 and 3 show the displacement between neighbouring atoms measured relative to the perfect crystal and with the magnitude of the arrow indicating the amount of either edge-like or screw-like displacement for the fully relaxed dislocation geometry [24]. The full colour contours in figures 2 and 3 show the linear-interpolated Nye tensor density, following the formulation of Hartley and Mishin [25], corresponding to the total $[1 1 -2 0]$ and $[1 -1 0 0]$ components in each case. Both edge and screw dislocations dissociate for the *ab initio* and Sun potential calculations, while only the edge dissociates for the Liu potential. The edge dissociation distances obtained from the $\langle 1 1 -2 0 \rangle$ component Nye tensor maps are $5.2a$, $4.5a$ and $4.0a$ (where $a \sim 3.2$ Å is the lattice parameter) for the *ab initio* calculations, Sun, and Liu potentials, respectively, as shown in table 3. The relative values of the splitting distances are in agreement with the relative values of the stable SFE. For the screw dislocation, the *ab initio* and Sun potential predict the same splitting distance of $2.0a$ while the Liu potential predicts a compact core with a width of $\sim 0.4a$. Although both interatomic potentials have larger SFEs and smaller splitting distances than the previous Mg potentials [2, 7] ($\sim 10 \, \text{mJ m}^{-2}$ SFE and $10a$ edge dislocation splitting distances), the Sun potential predicts both core structures in good agreement with *ab initio* while the Liu potential does not.

We have calculated the apparent $T = 0$ K Peierls stresses for the Sun and Liu dislocations, as shown in table 3, by direct measurement of the value of the appropriate shear stress needed to
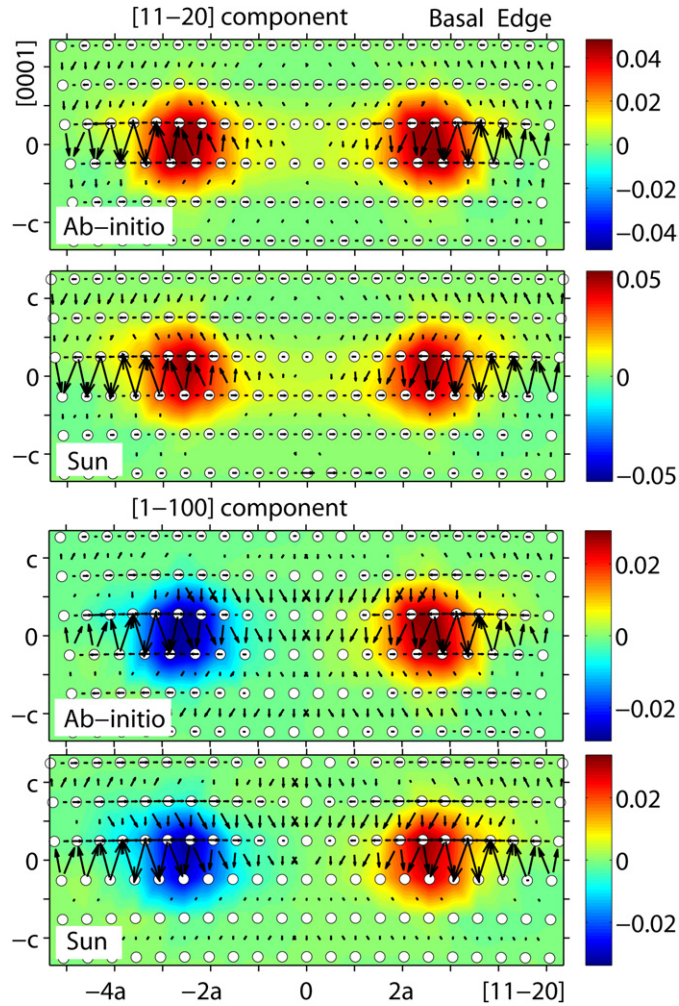
Figure 2. Basal edge $1/3\langle 1\,1-2\,0\rangle$ dislocation cores for *ab initio* calculations and Sun potential. The DD arrows and the Nye tensor colour map ($\langle 1\,1-2\,0\rangle$ and $\langle 1-1\,0\,0\rangle$ components) are superimposed.

move the dislocation from its initial position. Calculation of the true Peierls stress can be subtle, particularly when those stresses are small and when the simulation cells are small and fully periodic [26]. For a single dislocation in the centre of a simulation box of in-plane dimensions $d \times d$ with free surfaces, as used here, the spurious stresses acting on the dislocation as it moves by one Burgers vector along the glide plane due to image forces can be estimated using isotropic linear elasticity as $\tau_{\mathrm{img}} \sim \mu b^2/\pi d^2$. For our simulations, $d \sim 100$ nm, $b = a = 3.2$ Å and $\mu \sim 19$ GPa for shear along the basal plane, so that $\tau_{\mathrm{img}} \sim 0.6$ MPa. Computed Peierls stresses at this level are thus not reliable, but our results are somewhat larger. Specifically, we find both edge and screw dislocations of the Sun potential have low Peierls stresses of 0.3 MPa and 3.6 MPa, respectively, that are comparable to the experimental critical resolved shear stress for flow of $\sim$0.5 MPa [27]. In contrast, the Peierls stresses with the Liu potential are an order of magnitude larger, 14 MPa and >68 MPa for edge and screw dislocations, in some disagreement
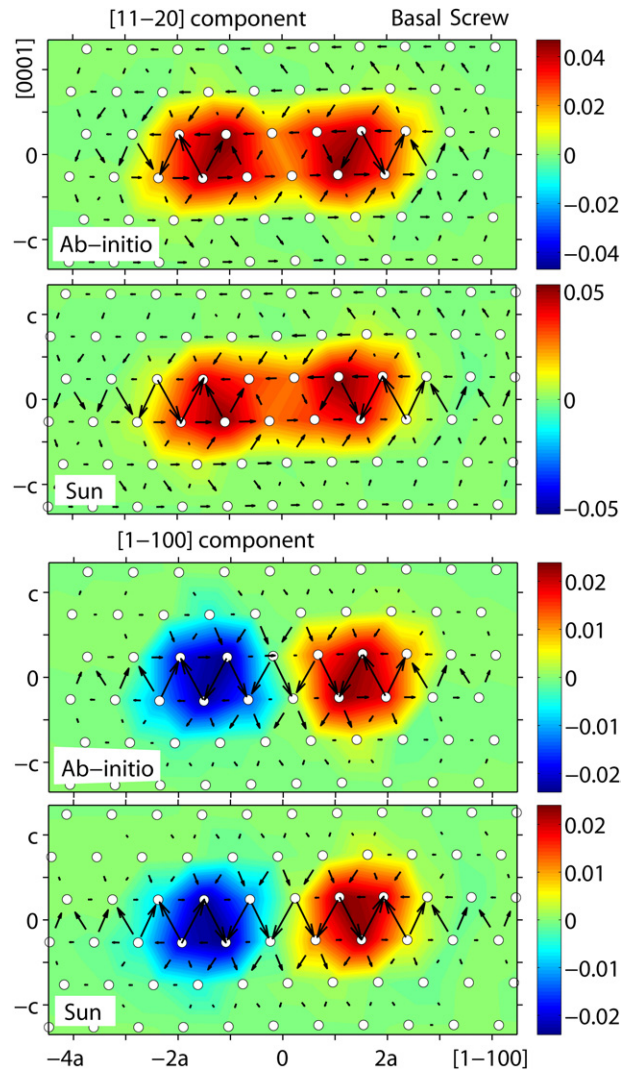
6

Figure 3. Basal screw $1/3\langle 1\,1\,{-}2\,0\rangle$ dislocation cores for *ab initio* calculations and the Sun potential. The DD arrows and the Nye tensor colour map ($\langle 1\,1\,{-}2\,0\rangle$ and $\langle 1\,{-}1\,0\,0\rangle$ components) are superimposed.

with the experiment. Since the Liu screw dislocation is not dissociated, the path to go from one Peierls valley to the other is along the $\langle 1\,1\,{-}2\,0\rangle$ direction that has a 240 mJ m^{-2} unstable SFE that induces a high Peierls stress. As the stress increases up to 68 MPa, the dislocation constricts and cross-slips onto the prism plane, where the dislocation energy and Peierls stress are lower, as seen in the next section.

4. Results for prism plane slip

The prism plane gamma surfaces are shown in figure 4 for all models. The *ab initio* calculation shows no stable SF. A stable SF is observed for both EAM potentials, but at different slip

Table 3. Various computed dislocation properties using *ab initio* and EAM methods. Difference ΔE_{core} between basal and prism core energies per unit length; dislocation dissociation distances as determined by the Nye tensor; and Peierls stresses. The dissociation distances are identified by the local extrema in the Nye tensor distribution (see figures 2, 3, 6, 7).

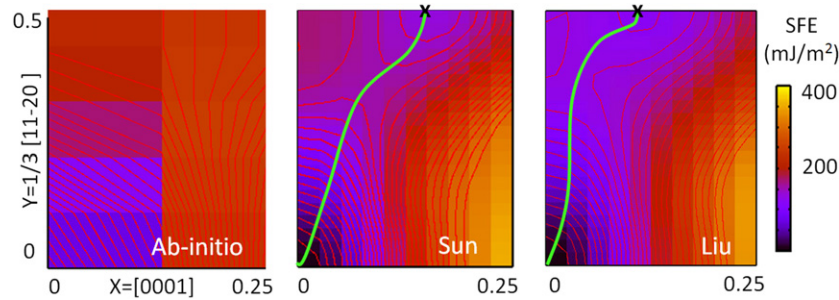| | ΔE_{core} (Basal–Prism) (eV/a) | | Dissociation distance | | | | Peierls Stress (MPa) | | | |
| | | | Basal | | Prism | | Basal | | Prism | |
	E	S	E	S	E	S	E	S	E	S
Ab initio			5.2a	2.0a	1.0a	X				
Sun EAM	−0.2	−0.03	4.5a	2.0a	1.0a	0.7a	0.3	3.6	13	44
Liu EAM	+0.13	+0.06	4.0a	0.4a	1.0a	0.7a	14	>68	15	44

Figure 4. Projections of gamma surfaces in the prism plane with $10\,\mathrm{mJ\,m^{-2}}$ isolines for *ab initio* calculations, Sun and Liu potentials. The paths of minimum energy are shown as green lines for the Sun and Liu potentials.

vectors ($1/6\langle 1\,1\,{-}2\,1\rangle$ for Sun and $1/6\langle 1\,1\,{-}2\,0.6\rangle$ for Liu) as indicated by the X in the figures. Figure 5 shows the values of the gamma surfaces along the $[1\,1\,{-}2\,0]$ direction and along the minimum energy path for each case. The unstable SFEs along the minimum energy path for the $\langle 1\,1\,{-}2\,0\rangle$ Burgers vector are given in table 2 and are much larger than in the basal plane. The Sun potential is again in better agreement with the *ab initio* calculations than is the Liu potential. However, since the unstable and stable SFEs are large, the dislocation cores are compact and so the existence of a stable SF has little effect on the dislocation core structures.

The prism plane edge and screw dislocation core structures are shown via DD plots and Nye tensor contours in figures 6 and 7, while the core-splitting distances obtained using the Nye tensor contours are shown in table 3. All the dislocation cores are compact and all edge cores are very similar with a width smaller than a. However, during the relaxation process in the *ab initio* calculations of the screw dislocation, the core recombines and cross-slips onto the basal plane while the Sun and Liu potentials predict a stable prismatic screw core of width $0.7a$. The Nye tensor contours for the Liu potential show slightly more dissociation than those for the Sun potential, in agreement with the lower stable and unstable SFEs for the Liu potential. The absence of a metastable prismatic screw dislocation in *ab initio* suggests the need for a driving stress on the prismatic plane for stability, and is compatible with the larger observed Peierls stresses for prismatic dislocations in Mg.

The Peierls stresses predicted using the Sun potential for the edge and screw dislocations are 13 and 44 MPa, about 10 times larger than the values obtained for the basal plane and
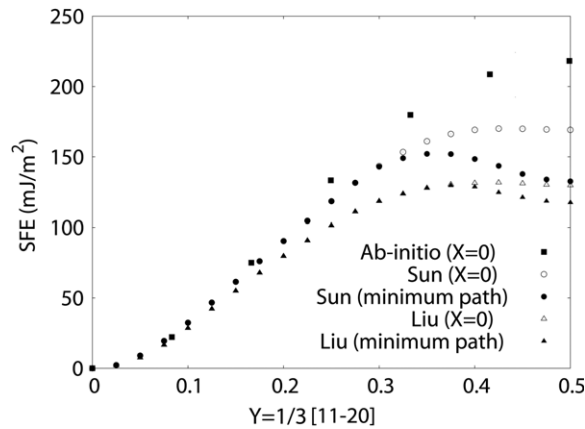
Figure 5. SFE in the prism plane as a function of the $\langle 1\,1\,-2\,0 \rangle$ component of the SF vector t (b), along the $Y = [1\,1\,-2\,0]$ direction ($X = 0$, open marks) and along the path of minimum energy (filled marks) for *ab initio* calculations (square), Sun (circle) and Liu (triangle) potentials.
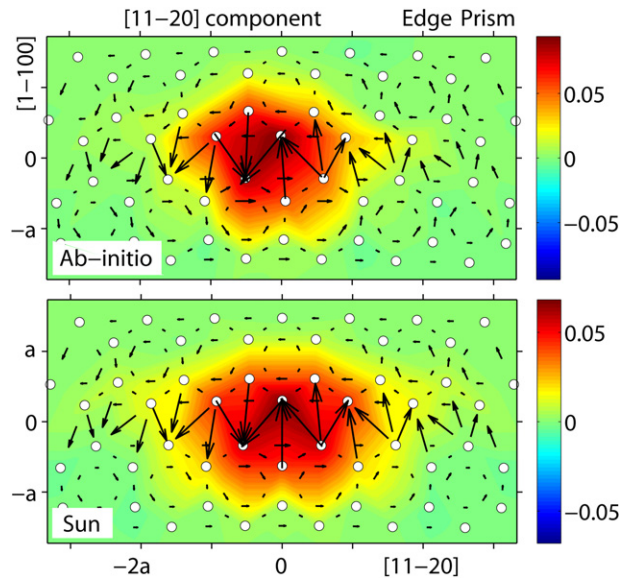

Figure 6. Prism edge $1/3\langle 1\,1\,-2\,0 \rangle$ dislocation cores for *ab initio* calculations and Sun potential. The DD and the Nye tensor colour map ($\langle 1\,1\,-2\,0 \rangle$ component) are superimposed.

in rough agreement with values of $\sim$40 MPa observed in experiments [27]. The Peierls stresses for the Liu potential are in the same range, 15 and 44 MPa for edge and screw, respectively, whereas the previously used na56 potential Peierls stresses are much too large, 54 MPa and 895 MPa, respectively. Thus, the anisotropy in Peierls stress (prism versus basal) is much higher for the Sun potential than for the Liu potential, with the Sun potential being more consistent with experiments. The Peierls stresses in the prism plane for both EAM potentials are likely underestimates since the *ab initio* calculations show a larger unstable SFE.
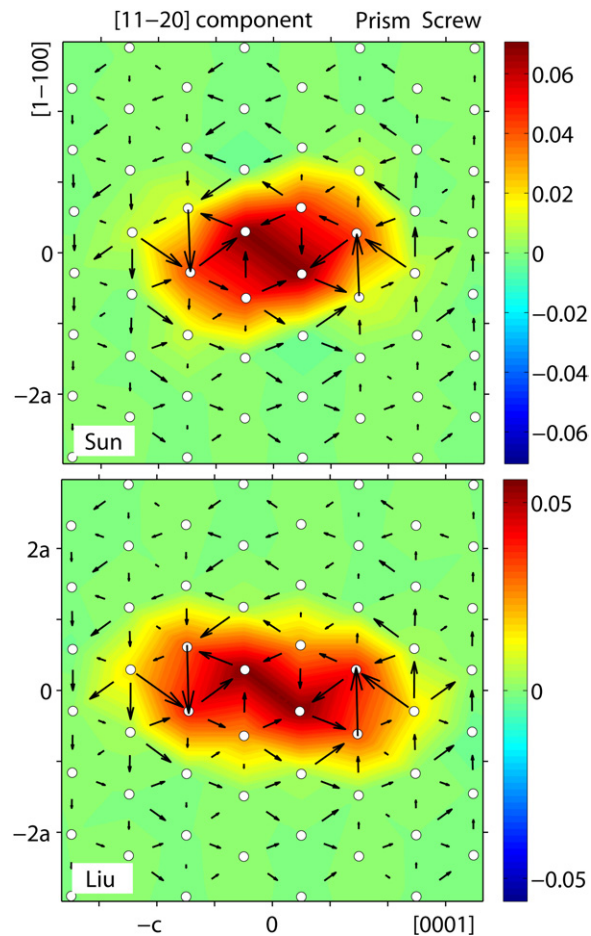
Figure 7. Prism screw $1/3\langle 1\,1\,-2\,0\rangle$ dislocation cores for Sun and Liu potentials. The DD and the Nye tensor colour map ($\langle 1\,1\,-2\,0\rangle$ component) are superimposed.

5. Discussion and conclusions

With detailed information on the predicted structures and energetics of the basal plane dislocations in section 3 and the prism plane dislocations in section 4, we now make some comparisons between basal and prism plane $\langle a\rangle$-type dislocations.

Differences in the predicted unstable SFEs for the prism plane are significant and should lead to differences in dislocation stability and Peierls stresses. The ratios between basal and prism unstable SFEs, an indicator of dislocation stability in the basal plane versus the prism plane, are 0.42 (*ab initio*), 0.62 (Sun) and 0.91 (Liu). These indicate a higher stability for basal dislocations in all cases, but with far less relative stability for the Liu potential. To further understand the relative stability of prism and basal dislocations as predicted by the two EAM potentials, we have estimated the dislocation core energies. Extracting core energies accurately is again subtle [26]. Here, we are interested in comparing energies between dislocations on different slip systems (basal and prism) but with the same Burger's vector. Because the Burger's vector is the same, the long-range elastic energies and spurious energies from image forces
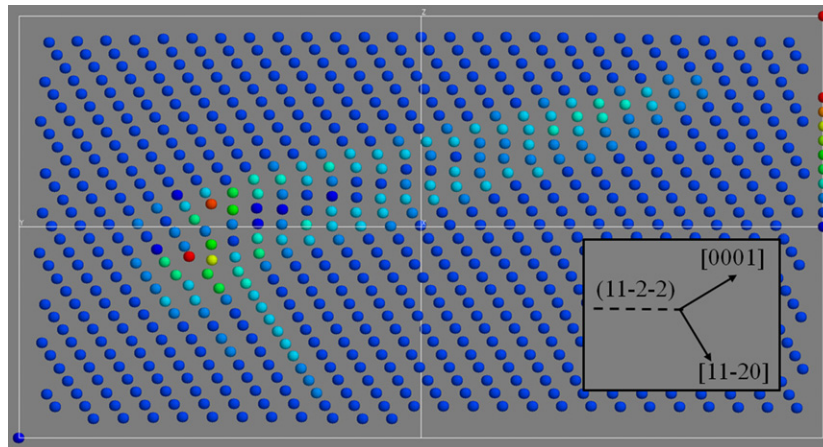
Figure 8. Edge $1/3\langle 1\,1\,{-}2\,3\rangle$ dislocation core in the $(1\,1\,{-}2\,{-}2)$ pyramidal II plane for Sun potential. The colour of atoms represents the atomic energies, with scale on the right ranging from -0.037 eV (dark blue) to 0.251 eV (red).

differ only due to elastic anisotropy. Thus, relative core energies can be obtained by examining the variation in the total deformation energy within a cylindrical region of radius r centred on the dislocation line as a function of the radius r. Here, the deformation energy of any region is defined as the total potential energy of the region in the deformed state minus the potential energy of the same number of atoms in the perfect crystal. For all four dislocations (edge and screw using Sun and Liu potentials), we find that beyond a rough 'core radius' of $r_{\rm c} = 2.0$ times the dissociation distance, the deformation energy per unit line length of dislocation scales as $E(r) = E(r_{\rm c}) + A \ln(r/r_{\rm c})$, with A is a potential-dependent constant. This scaling, which holds out to large r where boundary effects enter, is as expected from isotropic elasticity and indicates small elastic anisotropy effects. We can thus compute the difference in core energies $\Delta E_{\rm core} = E^{\rm basal}(r) - E^{\rm prism}(r)$ between basal and prism $\langle a \rangle$ dislocations at any radius $r > r_{\rm c}$. The resulting $\Delta E_{\rm core}$ values are shown in table 3 for both Sun and Liu potentials. For the Sun potential, the estimated basal core energy is smaller than the prism core energy while for the Liu potential it is greater; the energy differences between the prism and basal planes are -0.2 eV/a and -0.03 eV/a for Sun edge and screw dislocations, $+0.13$ eV/a and $+0.06$ eV/a for Liu edge and screw. This correlates with the unusual cross-slip of the screw dislocation from the basal onto the prism plane for the Liu potential.

In summary, we conclude that the Sun potential is in overall better agreement with *ab initio* calculations than the Liu potential. Its stable and unstable SFEs in the basal and prism planes and ratio of prism/basal unstable SFEs are closer to the *ab initio* values. The Liu potential also exhibits some unphysical properties: dislocations are more stable in the prism plane, the screw dislocation is not stable in the basal plane, and the Peierls stress for the basal edge dislocation is an order of magnitude too large. In contrast, the Sun potential provides satisfying dislocation properties in all cases: the screw dislocation is stable in both the basal and prism planes, but more stable in the basal plane, the dislocation core structures are very similar to those in the *ab initio* studies, and the Peierls stresses in the basal plane are low and 10 times smaller than in the prism plane, in qualitative agreement with experiments. However, there are still non-negligible discrepancies between the Sun potential and the *ab initio* calculations: the differences in unstable and stable SFEs in the basal and prism planes vary between -22%

and +29%, and the ratio of prism/basal unstable SFEs is +48% larger. We conclude that the Sun potential is more promising for the investigation of more-complex dislocation cores, and in particular the $\langle c + a \rangle$ cores that are crucial in Mg deformation. Figure 8 shows one of the stable core structures predicted by the Sun potential at zero applied load for a $\langle c + a \rangle$ edge dislocation in a $(1\,1-2-2)$ pyramidal II plane. The dislocation dissociates into two partials, one expanding in the basal plane and the other creating a $(1\,1-2\,1)$ twin embryo that extends over 40 Å. We will describe more details about the $\langle c + a \rangle$ dislocations and their behaviour under various applied loads in a separate publication, but Figure 8 suggests that the true core structure is too large to be studied by *ab initio* methods within current computational limits. Since the structure and behaviour of these dislocations must also be investigated as a function of applied loading, in particular for both compression and tension along the $\langle c \rangle$ axis, such depth of investigation remains beyond the ability of *ab initio* methods.

Acknowledgments

References

[1]   Kainer K U 2000 *Magnesium Alloys and Their Applications* (Weinheim: Wiley-VCH)
[2]   Basinski Z S, Duesbery M S and Taylor R 1970 *Can. J. Phys.* **48** 1480
[3]   Liang M H and Bacon D J 1986a *Phil. Mag.* A **53** 163
[4]   Liang M H and Bacon D J 1986b *Phil. Mag.* A **53** 181
[5]   Liang M H and Bacon D J 1986c *Phil. Mag.* A **53** 205
[6]   Serra A, Pond R C and Bacon D J 1991 *Acta metall.* **39** 1469
[7]   Igarashi M, Khantha M and Vitek V 1991 *Phil. Mag.* B **63** 603
[8]   Vitek V and Igarashi M 1991 *Phil. Mag.* A **63** 1059
[9]   Liu X-Y, Adams J B, Ercolessi F and Moriarty J A 1996 *Model. Simul. Mater. Sci. Eng.* **4** 293
[10] Sun D Y, Mendelev M I, Becker C A, Kudin K, Haxhimali T, Asta M and Hoyt J J 2006 *Phy. Rev.* B **73** 024116
[11] Ercolessi F and Adams J B 1994 *Europhys. Lett.* **26** 583
[12] Tewary V K 1973 *Adv. Phys.* **22** 757
[13] Sinclair J E, Gehlen P C, Hoagland R G and Hirth J P 1978 *J. Appl. Phys.* **49** 3890
[14] Woodward C and Rao S 2002 *Phys. Rev. Lett.* **88** 216402
[15] Trinkle D R 2008 *Phys. Rev.* B **78** 014110
[16] Yasi J A and Trinkle D R in preparation
[17] Woodward C, Trinkle D R, Hector L G Jr and Olmsted D L 2008 *Phys. Rev. Lett.* **100** 045507
[18] Bitzek E, Koskinen P, Gahler F, Moseler M and Gumbsch P 2006 *Phys. Rev. Lett.* **97** 170201
[19] Kresse G and Hafner J 1993 *Phys. Rev.* B **47** 558
[20] Kresse G and Furthmüller J 1996 *Phys. Rev.* B **54** 11169
[21] Vanderbilt D 1990 *Phys. Rev.* B **41** 7892
[22] Kresse G and Hafner J 1994 *J. Phys. Condens. Matter* **6** 8245
[23] Perdew J P and Wang Y 1992 *Phys. Rev.* B **45** 13244
[24] Vitek V 1974 *Cryst. Latt. Defects* **5** 1
[25] Hartley C S and Mishin Y 2005 *Acta Mater.* **53** 1313
[26] Bulatov V V and Cai W 2006 *Computer Simulations in Dislocations* (New York: Oxford University Press)
[27] Tonda H and Ando S 2002 *Metall. Mater. Trans.* A **33** 831
[28] Datta A, Waghmare U V and Ramamurty U 2008 *Acta Mater.* **56** 2531

[29] Jelinek B, Houze J, Kim S, Horstemeyer M F, Baskes M I and Kim S-G 2007 *Phys. Rev* B **75** 054106
[30] Smith A E 2006 *Surf. Sci.* **601** 5762
[31] Uesugi T, Kohyama M, Kohzu M and Higashi K 2003 *Mater. Sci. Forum* **419–422** 225
[32] Gotsis H J and Papaconstantopoulos D A and Mehl M J 2002 *Phys. Rev.* B **65** 134101
[33] Chetty N and Weinert M 1997 *Phys. Rev.* B **56** 10844
[34] Legrand P B 1985 *Phil. Mag.* A **52** 83
[35] Couret A and Caillard D 1985 *Acta Metall.* **33** 1455
[36] Fleischer R L 1986 *Scr. Metal.* **20** 223
[37] Fleischer R L 1985 *J. Met.* **37** 16
[38] Devlin J F 1974 *J. Phys. F: Met. Phys.* **4** 1865